Available online at www.sciencedirect.com
SCIENCE DIRECT®
Journal of Power Sources 117 (2003) 45–60
JOURNAL OF POWER SOURCES
www.elsevier.com/locate/jpowsour

Performance of high-temperature polymer electrolyte fuel cell systems

R.K. Ahluwalia, E.D. Doss*, R. Kumar

Argonne National Laboratory, 9700 South Cass Avenue, Argonne, IL 60439, USA

Received 14 December 2002; accepted 24 December 2002

Abstract

Performance of gasoline reformed, polymer electrolyte fuel cell (PEFC) systems for transportation with a high-temperature solid membrane capable of operating at 150–200 °C is discussed. Particular emphasis is placed on system layout, ease of fuel reforming, overall system efficiency, specific weight of the power system, heat rejection and water recovery. These are assessed in terms of the primary system variables, i.e. the operating pressure, reforming temperature, water-to-fuel ratio in the fuel processor, and the stack temperature. It is found that the system efficiency and water recovery are intimately affected by whether the condenser is located to operate at the system operating pressure or at close to ambient pressure.

Keywords: High temperature membrane; Fuel cell system performance; Fuel processing; Heat rejection; Water recovery

1. Introduction

High-temperature solid-polymer electrolyte membranes capable of operating at 150–200 °C are at an early stage of development. These are being advanced as alternatives to Nafion-based solid-polymer electrolyte membranes that operate at less than 90 °C. One advantage of operating at higher temperatures is the reduced sensitivity of the electrocatalyst to carbon monoxide in the anode stream. Reduced CO sensitivity and higher temperature operation may make it possible to lower the loading of anode and cathode catalysts. This is important because studies indicate that the precious-metal (Pt and Ru) content of the electrocatalysts is the single largest contributor to the total estimated cost of Nafion-based polymer electrolyte fuel cell (PEFC) systems [1]. Also, the reduction in overpotentials at higher temperatures can potentially lead to improvement in current density and a lighter and more compact stack. Specific weight and volume of PEFC stacks are of concern when dealing with Nafion-based membranes.

Higher temperature operation can also facilitate the issues of thermal management and water recovery. The heat generated by irreversibilities in a low-temperature stack is generally transferred to a coolant at 50–60 °C. It becomes problematic to reject the waste heat from the coolant to air in a radiator if the ambient temperature is about 49 °C (120 °F). The automotive radiators in internal combustion engines are sized to reject heat at 49 °C ambient temperature. The problem becomes less acute if the stack operates at 150–200 °C so that the coolant temperature is allowed to rise to 80–90 °C as in internal combustion engines. A Nafion-based membrane must be maintained in a hydrated condition or its electrical conductivity suffers. The anode and cathode streams entering a low-temperature stack must be fully or partially saturated in order to prevent the membrane from drying out. For self-sufficiency, the process water used to humidify the inflowing streams must be recovered [2]. A high-temperature membrane (HTM) operating above the boiling point of water will presumably not require humidification because liquid water will not form within the stack at the operating temperature. Thus, only the process water used in reforming the hydrocarbon fuel needs to be recovered.

The purpose of this work is to assess the impact of a high-temperature membrane on the overall gasoline reformed pressurized PEFC system. A conventional Nafion-based membrane maintained at 80 °C within a PEFC stack is regarded as the reference [3]. The primary focus is on system configuration, system and fuel processor efficiencies, and issues of heat rejection and water recovery. Two types of high-temperature membrane PEFC system configurations are considered: a high-performance system in which the water used for fuel processing is recovered downstream of the expander and a compact system in which the process water is recovered upstream of the expander. The condenser

* Corresponding author. Tel.: +1-630-252-5967; fax: +1-630-252-1774.
E-mail address: doss@anl.gov (E.D. Doss).

0378-7753/03/$ – see front matter © 2003 Elsevier Science B.V. All rights reserved.
doi:10.1016/S0378-7753(03)00028-4

in the first case operates at atmospheric pressure and in the second case at the system pressure. Detailed simulations have been conducted with the GCtool [4] software to show how the membrane temperature affects the choice of the compressor discharge pressure and the steam-to-fuel ratio that maximizes the efficiency of the auto-thermal reformer. Some discussion is given on the relative sizes of the catalytic reactors and the heat exchangers in order to highlight the perceived advantages and disadvantages of incorporating a high-temperature membrane in the fuel cell system.

2. High-temperature membrane PEFC system

Fig. 1 shows a PEFC system configured to take advantage of the high temperature of the membrane. The fuel is gasoline represented as a synthetic blend of 26 species of composition shown in Table 1. The liquid fuel is vaporized in a heat exchanger (hx_vap) by the exhaust from the gas turbine (gl_1). It is reformed in an auto-thermal reactor ATR (form) with preheated air and superheated steam. Some of the sensible enthalpy in the reformate is used to preheat air and to superheat steam in counterflow heat exchangers. Two catalytic reactors, high-temperature water-gas shift (HTS) and low-temperature water-gas shift (LTS), reduce the CO content of the reformate and produce additional hydrogen. Both are staged and intercooled to maximize CO conversion. Process water may be added to the shift reactors to further enhance CO conversion. A boiler is interspersed between the shift reactors to cool the reformate from the HTS to the LTS temperatures and raise steam needed in the ATR. A counterflow heat exchanger (ref_cool) cools the reformate from the low-temperate shift reactor temperature to the stack temperature, while heating the process water coming from the water tank. The cooled reformate flows through the anode channels of the fuel cell stack (PEFC).

A single-stage compressor supplies cathode air to the PEFC stack and the combustion air to the ATR. The unconverted hydrogen and CO in the spent anode gas are burnt with the depleted cathode air in a catalytic tail gas burner (mx_burn). Excess steam produced in the fuel processor is mixed in with the combustion products (mx_gt) and expanded in the gas turbine to generate useful power.

All the process water used in the fuel reforming circuit ends up in the effluent from the gas turbine. For self-sufficiency, it is recovered in an air-cooled condenser (conden). The recovered condensate in sp_cond is stored in a water tank from where it is pumped and circulated in the process water loop.

The PEFC stack is water-cooled. The coolant circuit is separate from the process water loop. The waste heat picked

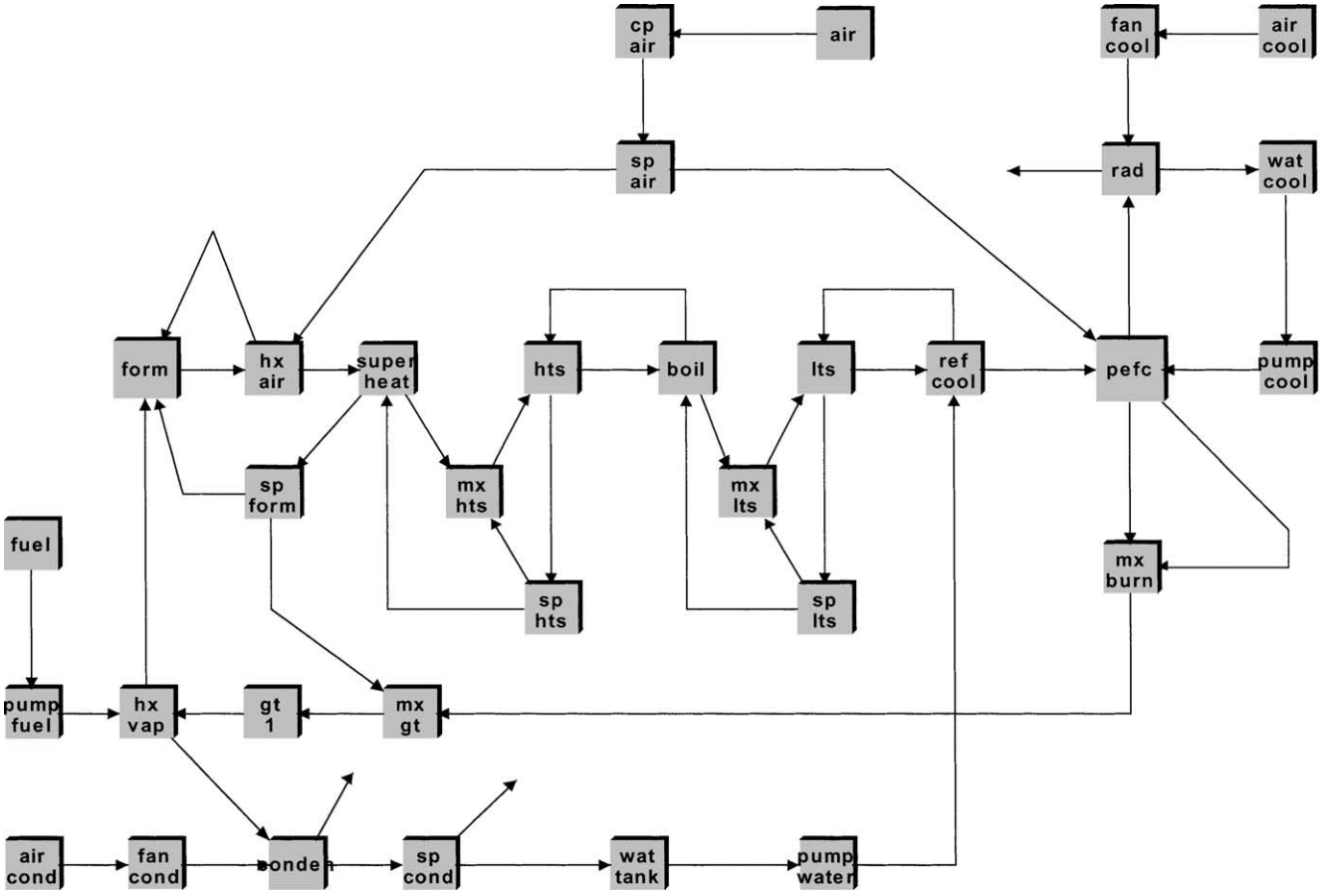

Fig. 1. Gasoline reformed PEFC system with a high-temperature membrane.

Table 1
Synthetic representation of gasoline

Formula	Mole fraction	Chemical name
C_4H_{10}-1	1.16	*N*-Butane
C_5H_{12}-1	13.19	*N*-Pentane
C_6H_{14}-4	5.91	2,2-Dimethylbutane
C_7H_{16}-5	7.77	2,3-Dimethylpentane
C_8H_{18}-13	31.26	2,2,4-Trimethylpentane
C_9H_{20}-4	4.58	2,2,5-Trimethylhexane
$C_{10}H_{22}$-1	1.01	*N*-Decane
$C_{11}H_{24}$	0.03	*N*-Undecane
$C_5H_{12}O$-2	9.82	2-Methyl-1-butanol
C_5H_{10}-4	1.45	*trans*-2-Pentene
C_6H_{12}-3	0.09	1-Hexene
C_5H_8-2	0.07	1,2-Pentadiene
C_5H_{10}-1	0.18	Cyclopentane
C_6H_{12}-2	0.74	Methylcyclopentane
C_7H_{14}-2	0.59	1,1-Dimethylcyclopentane
C_8H_{16}-1	0.22	1,1-Dimethylcyclohexane
C_8H_{18}-5	0.27	2,2-Dimethylhexane
C_9H_{18}-3	0.11	1-Nonene
$C_{10}H_8$	0.12	Naphthalene
$C_{11}H_{10}$-2	0.08	2-Methylnaphthalene
C_2H_4	0.26	Ethylene
C_6H_6	1.06	Benzene
C_7H_8	5.20	Toluene
C_8H_{10}-2	1.65	*M*-Xylene
C_9H_{12}-4	10.75	1-Methyl-3-ethylbenzene
$C_{10}H_{14}$-1	2.41	*N*-Butylbenzene

up by the coolant in the stack is rejected to the ambient air in a cross-flow radiator (rad).

Alternative configurations can be proposed for the high-temperature membrane system. The component layout can be selected for maximum performance, minimum weight or volume, compact stack or fuel processor, smallest condenser duty or size, or rapid startup. The layout shown in Fig. 1 is designed for maximum performance. In particular, the placement of the water-recovery condenser and the configuration of the process water loop are dictated by the goal of maximizing system efficiency.

3. System performance

Table 2 lists the parameter space over which the performance of the 50 kWe HTM system shown in Fig. 1 has been assessed. In order to limit the scope of this study, many of the parameters have been held at representative values. In particular, the cell voltage is selected to be 0.7 V, the fuel utilization in the PEFC stack is 85%, and the oxidant utilization is 50%. The specified temperatures of the shift reactors are typical of the midpoints of the operating range of the available catalysts. Steam superheat and the air preheat temperatures are somewhat aggressive but achievable. The isentropic efficiencies of the single-stage compressor and gas turbine are consistent with the DOE targets. For the low-temperature membrane (LTM) fuel cell system, the effects of system pressure, reforming temperature and water-to-fuel ratio in the ATR are discussed in detail by the authors in [5]. In this paper, similar study has been performed for the high-temperature membrane system and for different system configurations.

Table 2
Important parameters of the HTM system

System pressure (atm)	1.5–3.5
ATR temperature (K)	1100–1300
HTS temperature (K)	700
LTS temperature (K)	480
Ambient temperature (K)	300
Steam superheat temperature (K)	900
Air preheat temperature (K)	900
Stack temperature (°C)	150–200
Gas turbine efficiency (%)	90
Compressor efficiency (%)	75
Pump efficiency (%)	75
Fan efficiency (%)	75
Cell voltage (V)	0.7
Fuel utilization (%)	85
Oxidant utilization (%)	50
Water-to-fuel ratio in ATR (wt)	0.6–2.2
Water-to-fuel ratio in fuel processor (wt)	1.2–4

3.1. Water-to-fuel ratio

Fig. 2 shows the effect of water-to-fuel ratio (W/F) on the overall system efficiency (η_s). The results are shown as a function of both W/F in the ATR (β_A) and W/F in the complete fuel processor (β_F). At 1300 K reforming temperature, η_s is found to decrease with β_A. For $\beta_A = 0.6$, η_s increases as β_F is raised from 0.6 to about 1.7, reaches a maximum, and then decreases gradually as β_F is raised further. A similar trend is observed at $\beta_A = 1.2$. For β_A equal to 1.8 or higher, the system efficiency always decreases if any process water is added in the shift reactors.

The foregoing results suggests that at 1300 K reforming temperature and β_A less than 1.8, the optimum water-to-fuel ratio in the fuel processor is 1.8. For maximum efficiency, process water should be added to the reformate in the shift reactor such that β_F equals 1.8. Above $\beta_A = 1.8$, injection of water in the shift reactors is undesirable as it always lowers the system efficiency.

The system efficiency may be regarded as the product of the fuel processor efficiency (η_F) and the stack subsystem efficiency. Fig. 3 displays the variation of the fuel processor efficiency with water-to-fuel ratio. For the range of β_A considered in this study, at 1300 K reforming temperature, η_F increases with β_F but varies inversely with β_A. The dependence of η_F on β_F can be explained on the basis of CO concentration at the outlet of the LTS reactor. Each mole of CO in the reformate from the fuel processor represents a loss of potential H_2 that could have been formed by the following shift reaction:

$$CO + H_2O = CO_2 + H_2$$

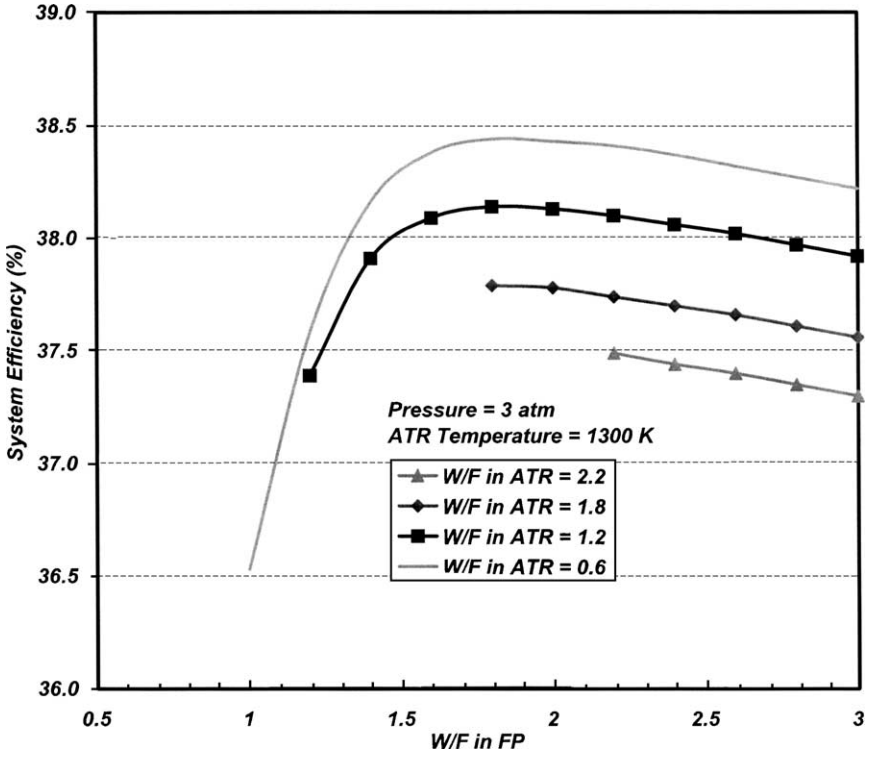

Fig. 2. Dependence of the optimum water-to-fuel ratio in the fuel processor on W/F in the ATR.

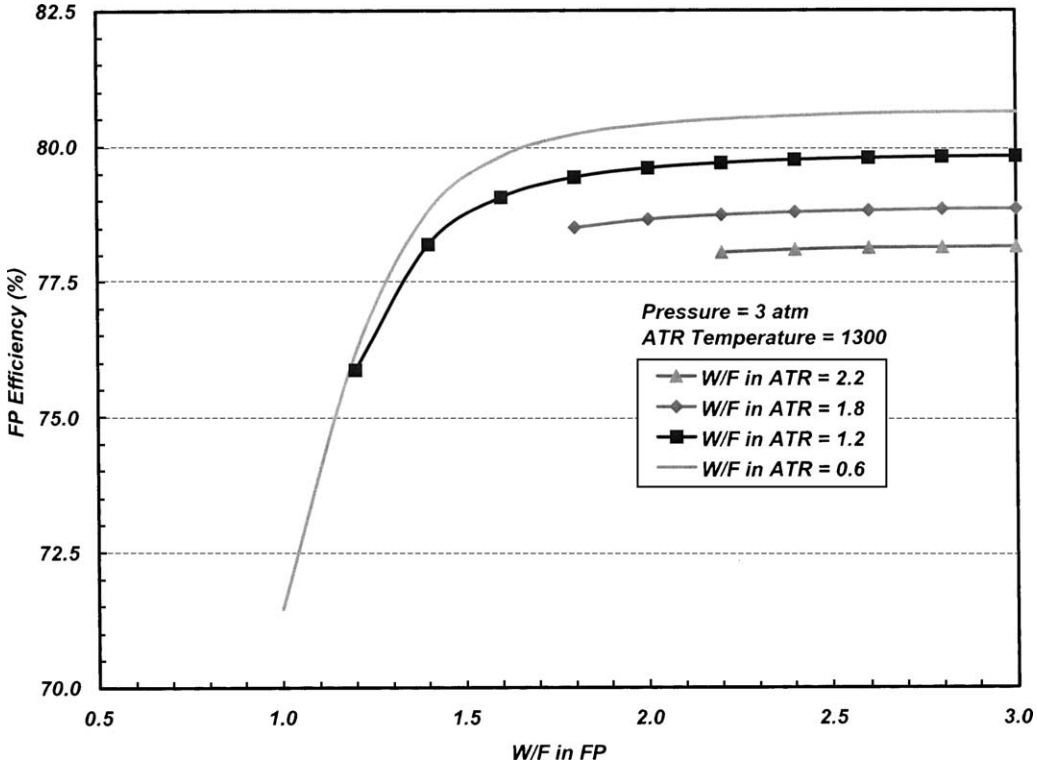

Fig. 3. Fuel processor efficiency as a function of water-to-fuel ratio in the fuel processor and the reformer.

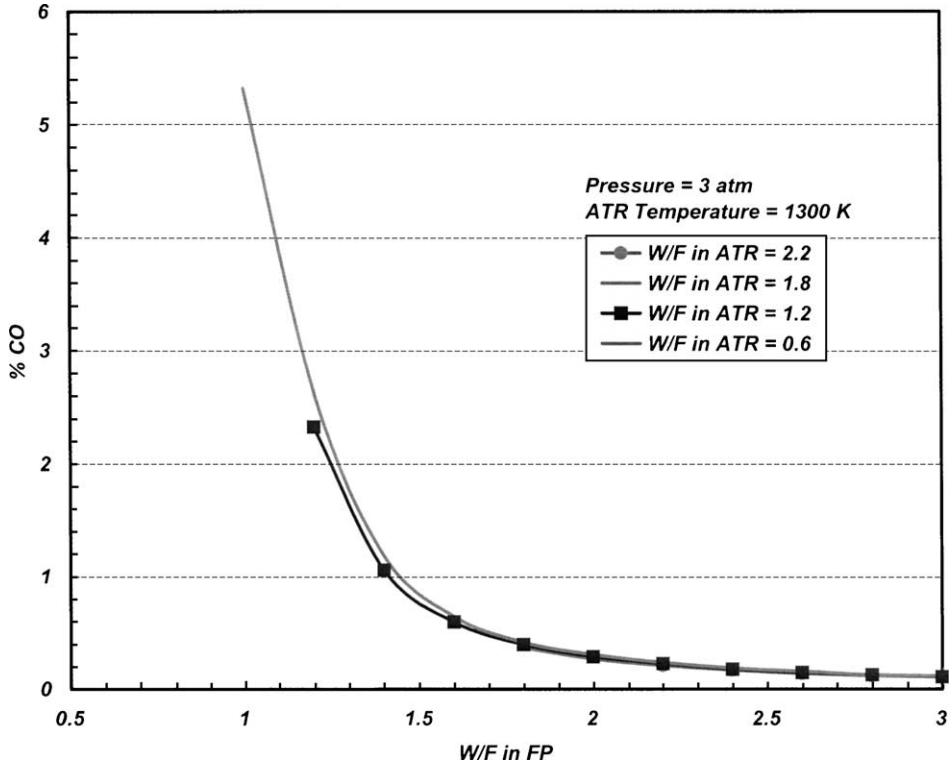

Fig. 4. Effect of W/F in the fuel processor on CO concentration in the reformate.

Thus, the higher the CO concentration in the reformate, the smaller the H_2 content, and the lower the fuel processor efficiency. According to Fig. 4, CO concentration in the reformate is a function of β_F and is rather insensitive to β_A. Starting from 5.3% at $\beta_F = 1$, the CO concentration decreases to 1% at $\beta_F = 1.4$, 0.5% at $\beta_F = 1.7$, 0.4% at $\beta_F = 1.8$, 0.3% at $\beta_F = 2$, 0.2% at $\beta_F = 2.4$ and 0.1% at $\beta_F = 3$.

At 1300 K reforming temperature, the fuel processor efficiency decreases with β_A because of thermal effects. In our simulation, water is added to ATR as superheated steam at 900 K. As such it must be heated to the reformer temperature. The sensible enthalpy necessary to heat steam to 1300 K is indirectly provided by the exothermic oxidation of fuel in the ATR. As more water is introduced into the ATR, additional air must be brought in to partially oxidize more fuel. The amount of H_2 produced in the ATR depends on the degree to which fuel is converted by steam reforming rather than by partial oxidation. Thus, the fuel equivalence ratio (ϕ) is a measure of the maximum H_2 that can be generated in the fuel processor. The higher the ϕ, the higher the fuel processor efficiency. At 1300 K reforming temperature, ϕ decreases from 3.3 at $\beta_A = 0.6$ to 3.2 at $\beta_A = 1.2$, 3.1 at $\beta_A = 1.8$ and 3 at $\beta_A = 2.2$.

The results in Figs. 2 and 3 can be combined to infer how the stack subsystem efficiency η_{FC} is affected by the water-to-fuel ratio in the fuel processor. The significant observation is that whereas the system efficiency decreases with β_F for $\beta_F > 1.8$, the fuel processor efficiency increases monotonically, albeit slowly, in the range of β_F considered. Thus, the decrease in η_s for $\beta_F > 1.8$ must be due to a corresponding decrease in η_{FC}. The stack subsystem efficiency is difficult to calculate directly but is easy to deduce as η_s/η_F. The decrease in η_{FC} with β_F is attributed to the reduction in the amount of steam fed to the gas turbine through the splitter sp_form. Fig. 5 shows such a trend, where for example at $\beta_F = 1.2$, the excess water-to-fuel ratio decreases from 1.4 for $\beta_F = 1.4$ to 0.25 for $\beta_F = 3.0$. The conclusion is that for $\beta_F > 1.8$, the increase in stack power with β_F (due to additional H_2 production by the water-gas shift reaction) does not compensate for the corresponding decrease in the power produced in the gas turbine. The results presented here are for 1300 K reforming temperature.

Fig. 6 shows the effect of water-to-fuel ratio on the condenser heat duty. Notice that the plots in Fig. 6 are mirror images of the curves in Fig. 2 for system efficiency at the same water-to-fuel ratio in ATR. Thus, the condenser heat load (Q_C) correlates very well with the system efficiency. It implies that Q_C depends on β_A and β_F in the same way as does η_s. For $\beta_F > 1.5$, Q_C is only weakly dependent on the water-to-fuel ratio in the fuel processor. We thus reach a conclusion that the condenser heat duty changes by less than 1%, even though β_F is doubled from 1.5 to 3. The reason for this result is that as seen in Fig. 5, on doubling β_F from 1.5 to 3, the total water to be recovered in the condenser increases by only 16%. Independent of β_F, all

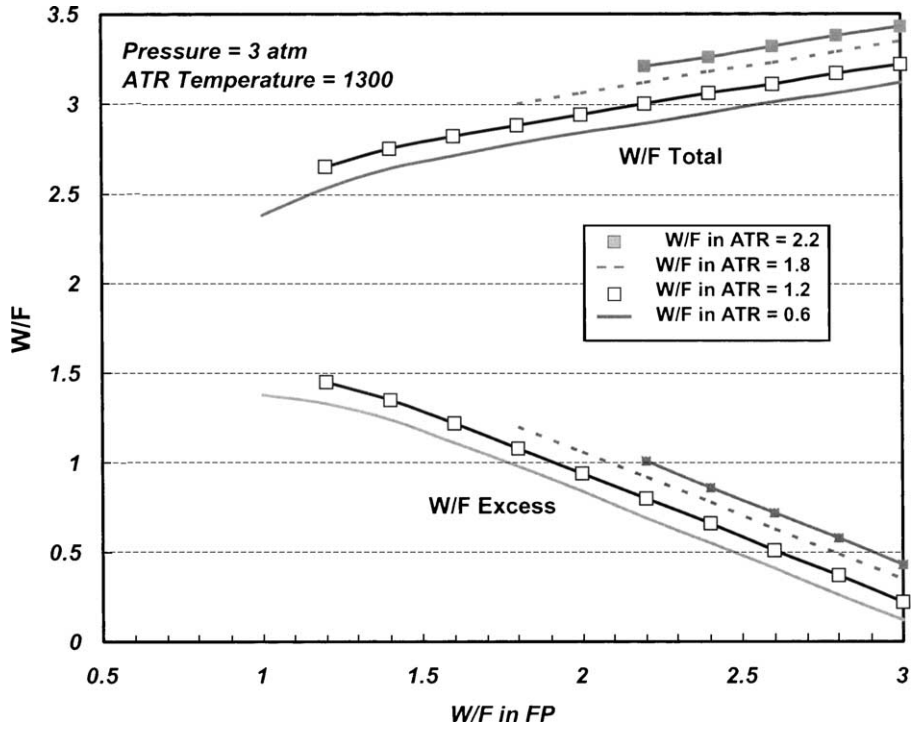

Fig. 5. Total, fuel processor, and excess W/F.

the water that is circulated in the process water circuit ends up in the combustion gas passing through the gas turbine. The water circulation rate is determined by the heat transfer loads on the reformate cooler, boiler, superheater, and low-temperature and high-temperature shift reactors. These loads in turn depend on the overall system efficiency rather than the amount of water that is injected in the fuel processor.

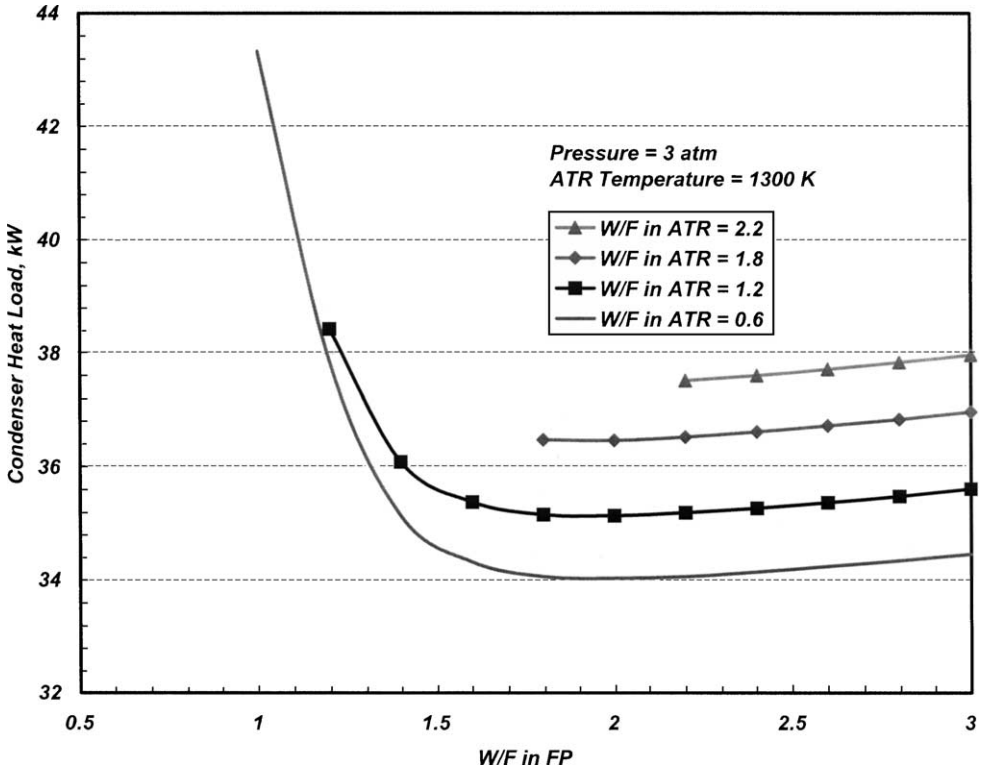

Fig. 6. Condenser heat load as a function of the water-to-fuel ratio in the reformer.

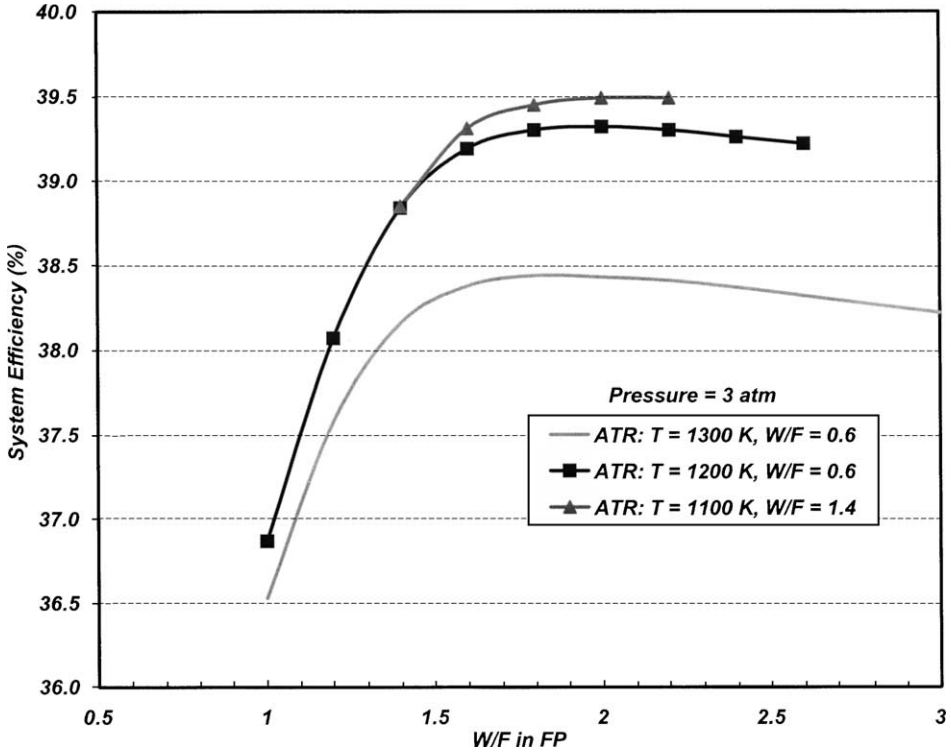

Fig. 7. Effect of reforming temperature on the system efficiency and the optimum water-to-fuel ratio in the FP and the ATR.

3.2. Reforming temperature

Fig. 7 shows the effect of the auto-thermal reformer exit temperature (T_{ATR}) on the overall system efficiency. The efficiencies are presented as a function of the water-to-fuel ratio in the fuel processor at three reforming temperatures. The water-to-fuel ratio in the ATR is selected to yield the highest system efficiency at the specified reformer exit temperature. At 1300 and 1200 K T_{ATR}, the system efficiency maximizes at the lowest β_A considered in this study, i.e. $\beta_A = 0.6$. At 1100 K T_{ATR}, the system efficiency is maximum at $\beta_A = 1.4$.

With respect to the water-to-fuel ratio in the fuel processor (β_F), the system efficiency is highest at $\beta_F = 1.8$ when the reformer temperature is 1300 K. As T_{ATR} is lowered, the optimum β_F tends to increase. The optimum β_F rises to 1.9 at 1200 K reformer exit temperature and to 2 at 1100 K T_{ATR}.

The increase in system efficiency with lowering of the reformer exit temperature is attributed to the improvement in the fuel processor performance. Corresponding to the optimum values of β_A and β_F, the fuel equivalence ratio increases from 3.3 at 1300 K T_{ATR} to 3.5 at 1200 K and 3.9 at 1100 K. As mentioned earlier, generally the higher the fuel equivalence ratio the better the fuel processor efficiency. At the optimum β_A and β_F, the fuel processor efficiency is 80.2% at 1300 K T_{ATR}, 82.6% at 1200 K and 84.8% at 1100 K T_{ATR}.

The problem of methane slip may be encountered as the reformer exit temperature is lowered. At 1300 K T_{ATR}, the methane concentration is less than 150 ppm (0.005%) in the entire range of β_A considered. Fig. 8 shows that the equilibrium CH_4 concentration in the reformate can exceed 5000 ppm (0.5%) at 1100 K T_{ATR} if $\beta_A = 0.6$. In accordance with the steam reforming reaction,

$$CH_4 + 2H_2O = CO_2 + 4H_2$$

this is equivalent to a potential 4 percentage point reduction in H_2 concentration for every percent of methane formation. As shown in Fig. 8, the tendency to form methane can be suppressed by adding steam in the ATR. Given that the CH_4 concentration decreases with β_A but more combustion air must be supplied to the ATR to provide the sensible enthalpy necessary to raise the temperature of the added steam to T_{ATR}. There is an optimum β_A at which the fuel processor efficiency is the highest. At 1100 K, the optimum β_A is about 1.4. Similar explanation for the effects of T_{ART}, methane formation, and W/F ratio are given in [5] for the low-temperature membrane system.

3.3. Operating pressure

A parametric study was conducted to investigate the effect of the operating pressure on the overall system efficiency. The results of this study are summarized in Fig. 9 for three values of reformer exit temperature. Water-to-fuel ratios in the ATR and in the fuel processor were varied independently to maximize the system efficiency for given operating pressure and specified reformer exit temperature. Thus, β_A and β_F are different for each data point. The optimum β_A was found to be 0.6 at T_{ATR} of 1300 and 1200 K for all

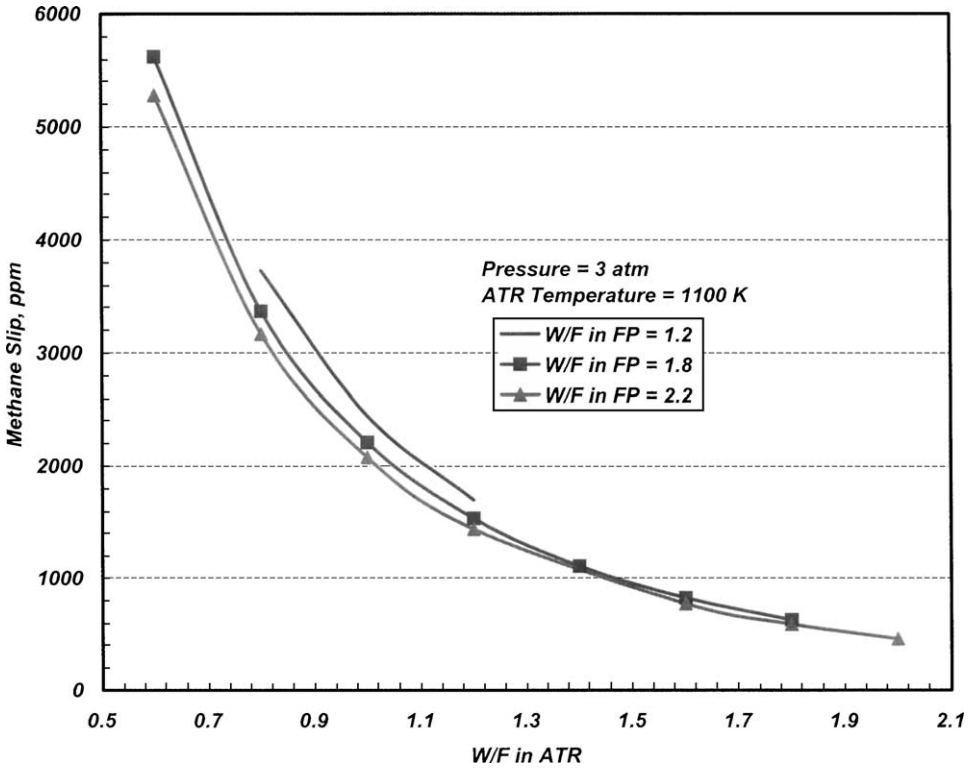

Fig. 8. Relationship between methane slip and water-to-fuel ratio in the auto-thermal reformer.

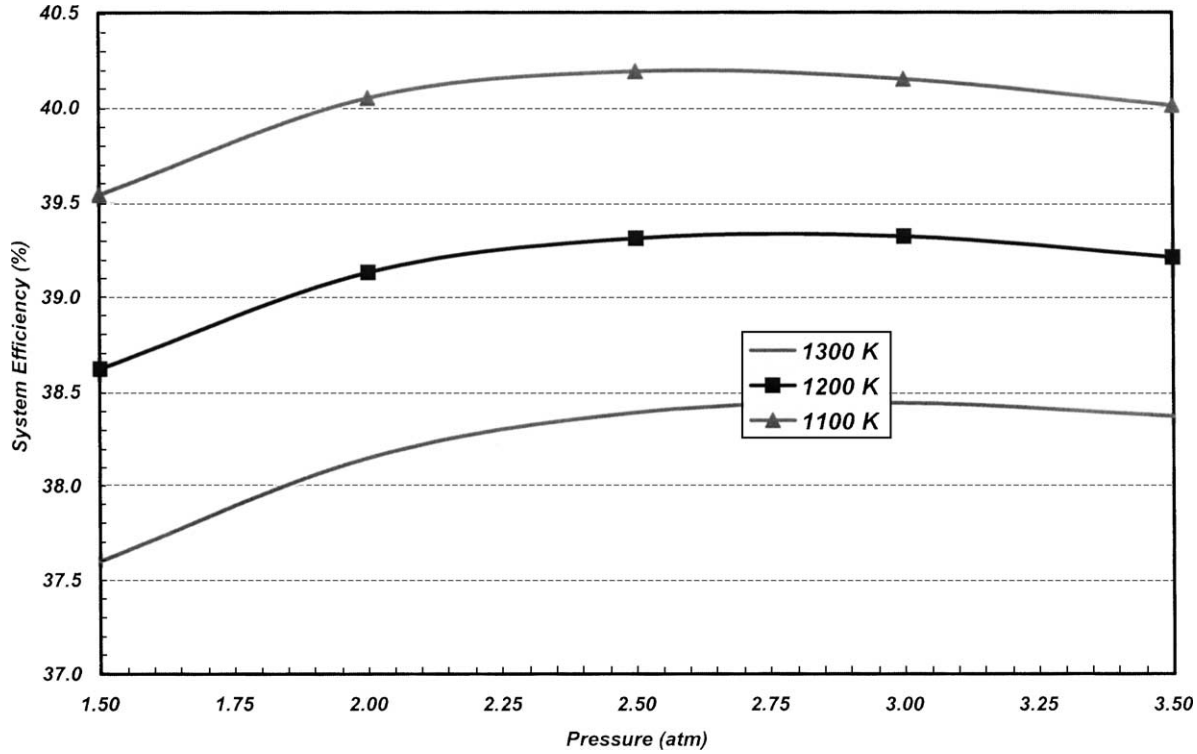

Fig. 9. Relationship between the optimum operating pressure and the ATR exit temperature.

levels of pressure. At 1100 K, the optimum β_A is between 1.4 and 1.8. Similarly, the optimum β_F was found to vary with pressure from 2.0 to 2.2 at 1100 K, from 1.8 to 2.2 at 1200 K, and from 1.8 to 2.6 at 1300 K reformer exit temperature.

Fig. 9 shows that for a specified reformer exit temperature, there exists an optimum operating pressure (and β_A and β_F) at which the system efficiency is highest. As the operating pressure is raised, the fuel processor becomes less efficient but the net power produced by the compressor-expender module (CEM) increases. At 1300 K reformer exit temperature, the fuel processor efficiency decreases from 80.7% at 1.5 atm to 80.1% at 3.5 atm whereas the net power generated by CEM increases from 1.8 to 3.1 kW. The two conflicting trends result in the system efficiency maximizing at an intermediate pressure of 3 atm. Fig. 9 also shows that the optimum pressure increases with the reformer exit temperature. It is 2.5 atm at 1100 K T_{ATR}, 2.75 atm at 1200 K and 3 atm at 1300 K. Also, the fraction of the net power that is produced by the CEM increases with T_{ATR} (see Fig. 10).

The operating pressure also affects the heat loads on the PEFC radiator (Q_R) and the process water condenser (Q_C). Fig. 11 shows that the radiator heat load increases with pressure because of the higher compressor discharge temperature. In our simulations of the high-temperature membrane system, the compressed air is directly fed to the PEFC cathode without heating or cooling it to the cell temperature. The reformer exit temperature has only a small influence on Q_R.

The condenser heat duty always decreases with the operating pressure but increases with the reformer exit temperature. As the system pressure is raised, the pressure ratio across the gas turbine increases causing the turbine exit temperature to go down. This implies a smaller heat load on the process water condenser. Fig. 11 shows a 22% reduction in heat duty if the operating pressure is raised to 3.5 from 1.5 atm. The corresponding reduction in the condenser size and weight is larger because much of the decrease in heat duty is due to the smaller sensible heat load. The sensible cooling in the desuperheating section of the condenser involves gas-to-gas heat exchange for which the overall heat transfer coefficient is small compared to that for the condensing section where phase change occurs.

3.4. Cell temperature

Fig. 12 displays the effect of cell temperature on the overall system efficiency as a function of system pressure. Here the water-to-fuel ratio in the ATR is fixed at 0.6 which is the optimum for 1200 K reformer exit temperature, whereas that for fuel processor (β_F) has been determined parametrically for highest efficiency. Depending on the cell temperature and the operating pressure, β_F varies between 1.8 and 2.4.

Fig. 12 indicates that the system efficiency improves with the cell temperature (T_{FC}). Note that the cell voltage is fixed at 0.7 V so that the stack efficiency actually declines slightly with T_{FC}. The PEFC stack efficiency is 55.6% at 150 °C and

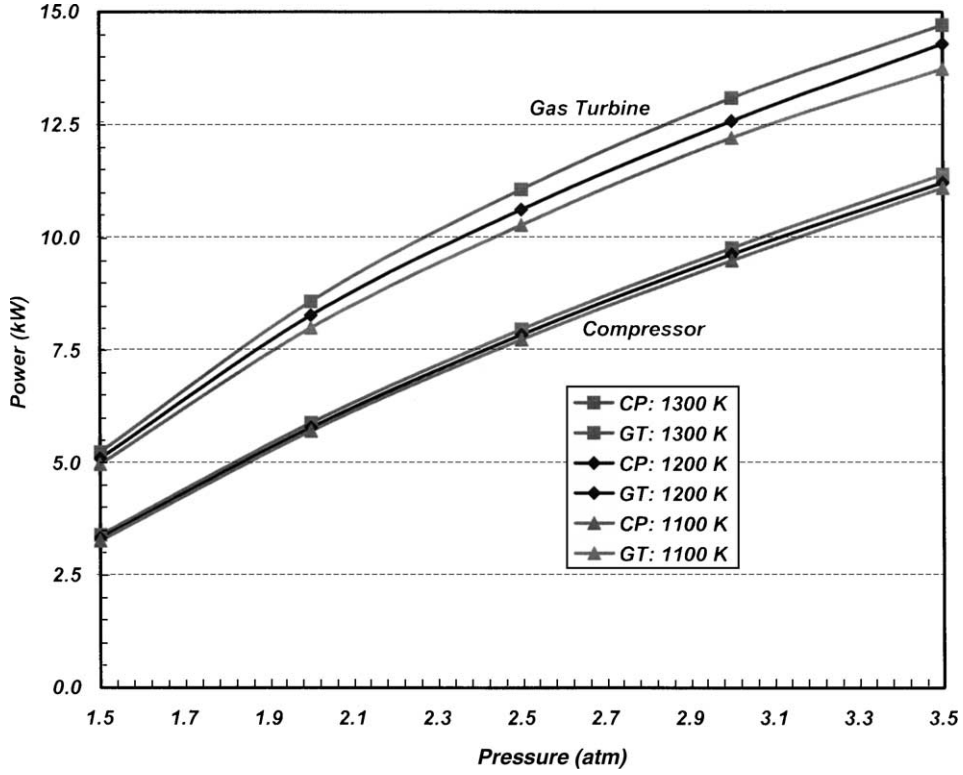

Fig. 10. CEM performance as a function of the operating pressure and the ATR exit temperature.

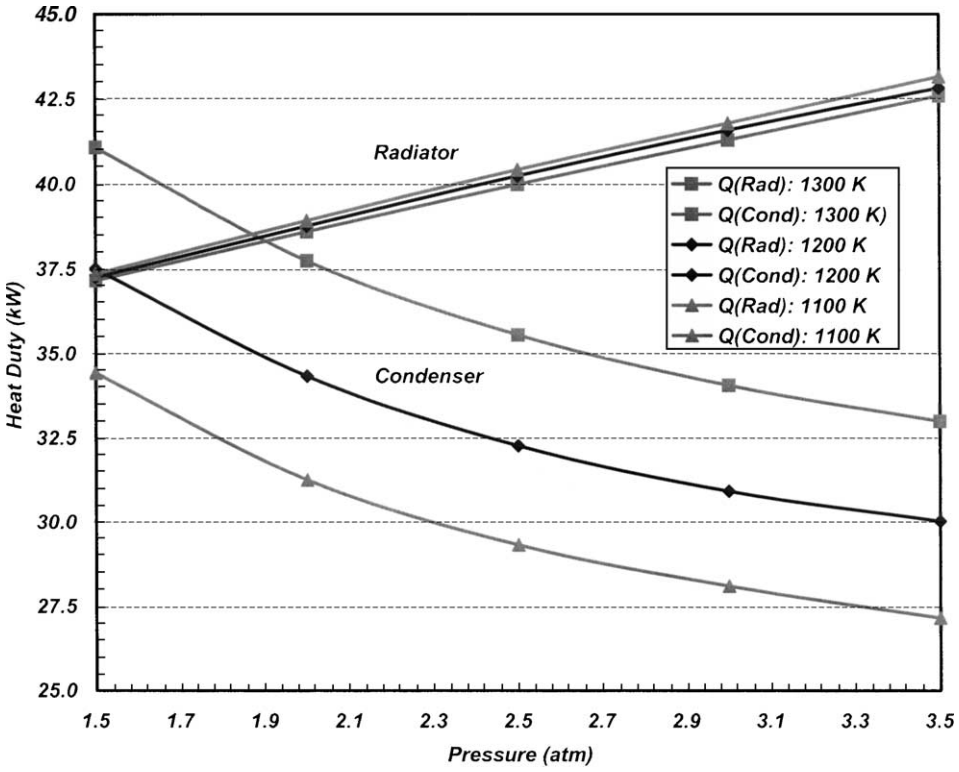

Fig. 11. Heat loads on the condenser and radiator as functions of the operating pressure and ATR exit temperature.

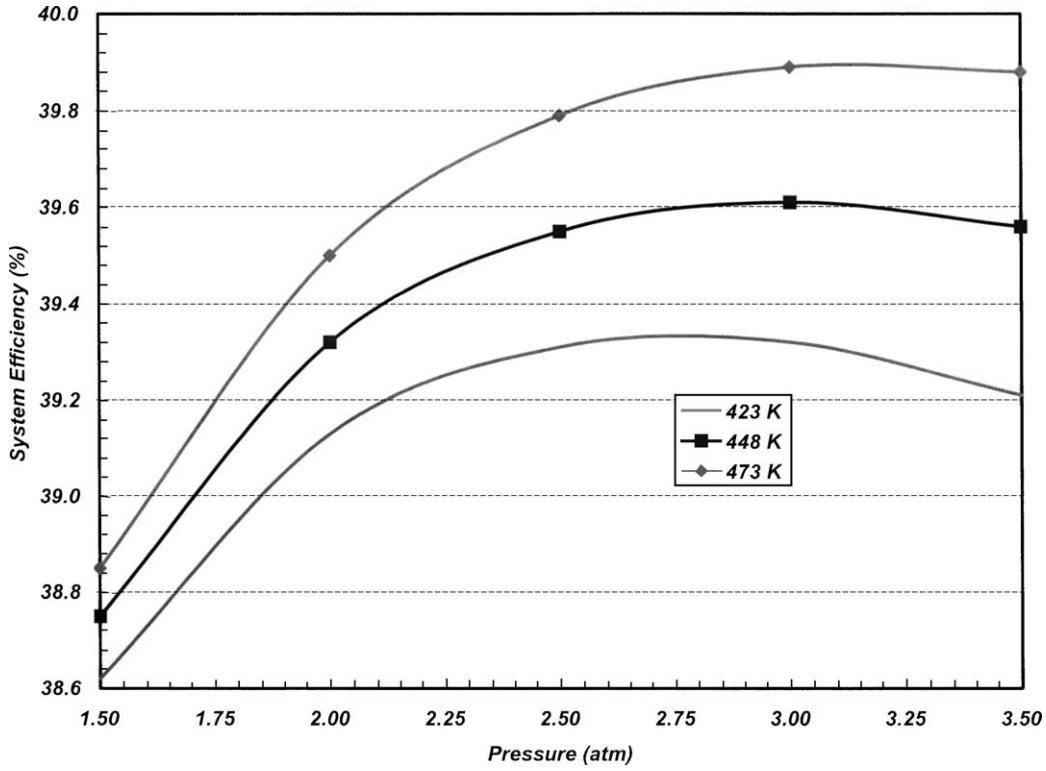

Fig. 12. Dependence of the optimum operating pressure on the stack temperature.

55.5% at 200 °C. Also, the fuel processor efficiency does not directly depend on T_{FC}. The increase in η_s with T_{FC} stems from the greater net power generated by the CEM. At 3 atm operating pressure, the turbine inlet temperature rises by 37 °C, from 360 to 397 °C, as the cell temperature is raised from 150 to 200 °C. This translates into a 0.5 kW increase in the net power generated by the CEM and a 0.6% improvement in the system efficiency.

For a given cell temperature, there is an operating pressure at which the system efficiency is highest. The optimum operating pressure increases with the cell temperature. At 1200 K ATR exit temperature, the optimum pressure is 2.75 atm at TFC of 150 °C, 3 atm at 175 °C, and 3.1 atm at 200 °C.

3.5. Low-temperature membrane

A parametric study was conducted to compare the performance of the HTM system with the LTM systems. The latter are configured around a Nafion like membrane that is assumed to operate at 80 °C. These include a preferential-oxidizer (PROX) catalytic bed located just downstream of the low-temperature shift reactor to reduce CO concentration to less than 10 ppm. A heat exchanger (ref_cool) is placed between the PROX reactor and the PEFC stack to cool the reformat to the cell temperature. Also, the compressor discharge that forms the cathode air is humidified with process water to cool it to the cell temperature.

We have considered three configurations of the low-temperature system. Fig. 13 shows a layout that is identical to the high-temperature system except for the PROX reactor, reformate cooler, cathode humidifier, and a heat exchanger to cool the reformate from 480 K, the LTS operating temperature, to 423 K, the PROX operating temperature. In the second configuration, the portion of the process water circulating through the reformate heat exchangers that is in excess of what is needed in the fuel processor is cooled in a condenser and returned to the water tank. This configuration was analyzed to determine the increase in system efficiency realized by expanding the excess steam in the gas turbine. The third configuration is the same as the second except that the condenser is relocated just downstream of the PEFC stack. The performance of the low-temperature membrane system with a pressurized condenser has been analyzed extensively in the past [6].

Fig. 14 summarizes the results of the parametric study for 1200 K ATR exit temperature. The results are presented as a function of the operating pressure. The water-to-fuel ratio in the ATR is 0.6 but differs in the fuel processor for the high-temperature and low-temperature systems. As before, β_{FP}

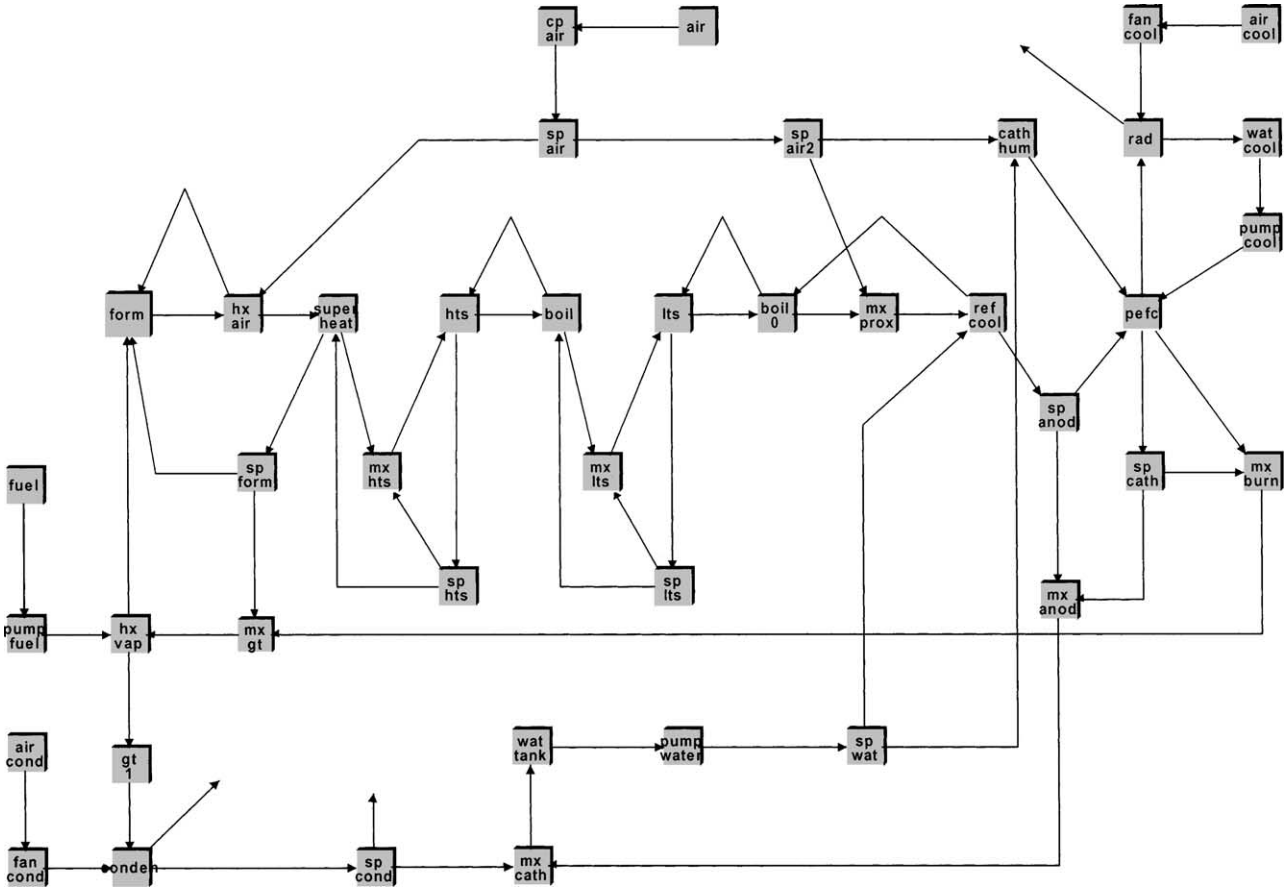

Fig. 13. Gasoline reformed PEFC system with a low-temperature membrane.

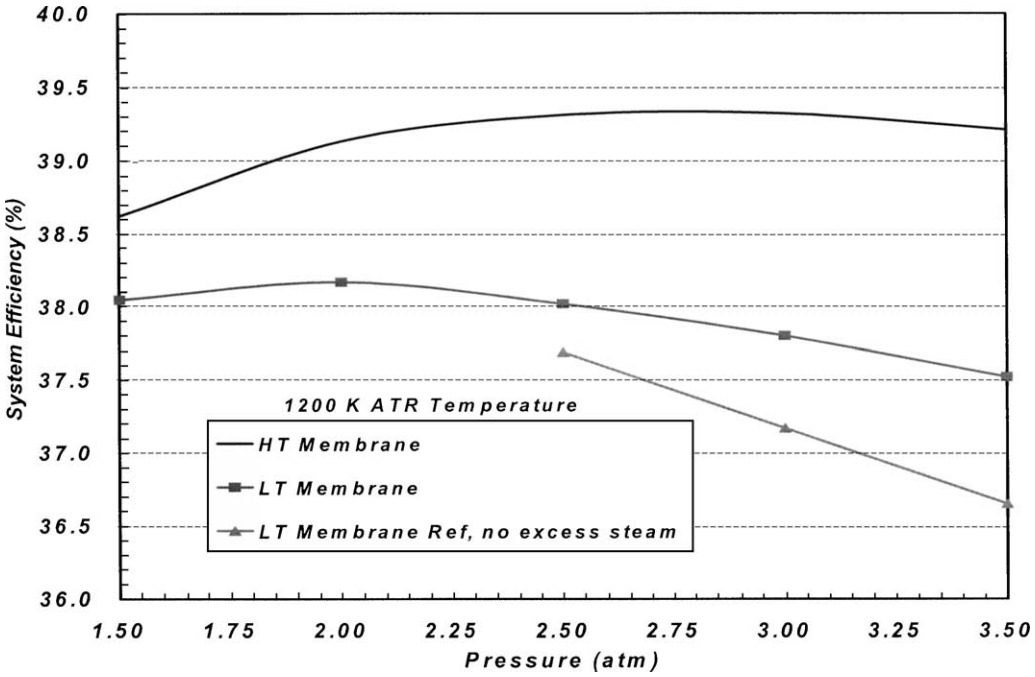

Fig. 14. Comparison of the system efficiencies of the HTM and LTM systems.

has been determined to yield the highest system efficiency. It lies between 1.8 and 2.2 for the 150 °C membrane system and between 3 and 3.2 for the 80 °C membrane system.

We first compare the two systems in which the excess steam produced in the fuel processor is injected into the gas turbine. It is seen that the 150 °C membrane system is always more efficient than the 80 °C system. The difference in the system efficiencies widens with the operating pressure, reaching 1.7% at 3.5 atm. The system efficiency of the 80 °C membrane system optimizes at 2 atm and of the 150 °C membrane system at about 2.75 atm. At the optimum points, the LTM system has an efficiency of 38.2% compared to 39.3% for the HTM system. The difference in system efficiency is due to the higher turbine inlet temperature: 360 °C for the HTM system versus 260 °C for the LTM system. As a result, the net power produced by the CEM in the LTM system is about 1.8 kW smaller (1.2 kW versus 3 kW for the HTM).

We next compare the two LTM systems with and without excess steam injected into the gas turbine. Without steam injection, the system efficiency monotonically decreases with the operating pressure and is 0.3–0.8 percentage points smaller than with excess steam injection. The reduced efficiency is obviously a result of poorer performance of the CEM. In fact, without excess steam injected into the gas turbine, the net power produced by the CEM module is negative, i.e. the air compressor consumes more power than generated by the gas turbine.

Finally, for completeness we quote results for a LTM system with a pressurized condenser between the PEFC stack and the gas turbine. This reference system does not have a provision for injection of excess steam into the gas turbine. At 1200 K reformer exit temperature, this system has a peak efficiency of 36.4% at 0.7 V cell potential. It is about 1.2 percentage point less than the efficiency of the equivalent LTM system with the condenser downstream of the gas turbine. The drop in efficiency is due to an increase in power consumption by the CEM.

4. Assessment of high-temperature membrane system

Cost, weight and volume are as important as the system efficiency. In this section, we offer a preliminary comparison of the weights of some important components and subsystems in the HTM and LTM systems. The subsystems considered are the fuel processor, the main heat-rejection radiator for the PEFC stack and the water-recovery condenser. Sufficient information is not available at this time to present a meaningful comparison of the PEFC stacks. It is clear however, that the very motivation for developing high-temperature membranes is to decrease membrane cost, reduce loading of electrocatalysts, and make the stack more compact by enhancing power density.

4.1. High efficiency system

Table 3 shows the gas hourly space velocities (GHSV) achieved under laboratory conditions and the specified DOE targets. The current GHSV data for the ATR catalyst is for a bifunctional precious-metal catalyst in the form of pellets. The GHSV target has been met with powders and microchannel structures in microreactor tests. The long-term goal is to improve the catalyst stability in a structured form and

Table 3
Estimated amounts of catalysts required in the HTM and LTM systems

System	ATR		Sulfur removal		WGS		PROX		Burner		Total	
	Current	Target	Current	Target	Current	Target	Current	Target	Current	Target	Current	Target
HTM system												
GHSV (h^{-1})	15000	200000	5000	50000	7500	45000	N/A	N/A	15000	200000	2100	19100
Volume (l)	5.1	0.4	15.4	1.5	13.2	2.2	N/A	N/A	5.1	0.4	38.8	4.5
Weight (kg)	8.1	0.6	24.6	2.5	21.2	3.5	N/A	N/A	8.1	0.6	62.0	7.2
LTM system												
GHSV (h^{-1})	15000	200000	5000	50000	5000	30000	10000	150000	15000	200000	1600	14300
Volume (l)	5.3	0.4	16.2	1.6	24.7	4.1	12.3	0.8	5.3	0.4	63.8	7.3
Weight (kg)	8.5	0.6	25.9	2.6	39.5	6.6	19.7	1.3	8.5	0.6	102.1	11.7

develop equally active non-noble metal catalysts. The GHSV data in Table 3 for sulfur removal has been obtained with ZnO pellets. Laboratory tests have demonstrated reduction of H_2S from 20 to 1.2 ppm with a ZnO-coated monolith at 1000 h^{-1} and 480 °C. A getter may be required to reduce H_2S concentration to ppb levels. The current data for WGS catalysts has been obtained with 0.5–1% Pt on a mixed oxide on alumina pellets. The longer-term goal is to develop a non-precious-metal, non-pyrophoric, WGS catalyst formulation applied on a monolith. The data for PROX is also with a palletized precious-metal catalyst although a monolith is the preferred form. Table 3 lists the projected catalyst requirements computed from the above values of GHSVs and the state points determined in our simulations. The projections are given for both the current and target GHSVs. Note that the GHSV for the WGS catalyst in HTM system is 50% higher because there is not as much incentive to reduce the CO concentration in LTS reactor to as low a level as in the LTM system. The equilibrium concentration of CO at LTS exit is 0.1% for the LTM system and 0.3% for the HTM system.

Table 3 indicates that in terms of the catalyst requirements, the fuel processor for the near-term HTM system can be nearly 40% lighter than that for the LTM system. The saving comes from higher GHSV for WGS catalyst and the elimination of the PROX reactor. With sulfur-free gasoline, the fuel processor for the HTM system is almost 60% lighter. If the targets GHSVs are attained, the catalyst weight is about 88% less than the near-term value for the HTM system.

For high efficiency, the fuel processor must be tightly integrated with the other components needed for preheating air, raising steam, and vaporizing fuel. Table 4 lists the heat duties on the air heater, process water heat exchangers within the fuel processor, and the fuel vaporizer. Also listed are the weights of these components estimated on the basis of assuming heat transfer coefficients of 50 W/(m^2 K) on the gas side and 100–1000 W/(m^2 K) on the sides with a liquid or a phase change. Note that the heat duty on the process water heat exchangers is about 60% higher for the LTM system but the weight is three times as large. The reformate cooler used in the LTM system to bring the anode stream to the cell temperature is responsible for the differences in heat duties and weights. It may be possible to reduce the sizes of heat exchangers with microchannel construction.

Combining the results in Tables 3 and 4 and allowing for 15% additional weight for catalyst containment, the specific weight of the fuel processor for the HTM system is estimated to be 1.5 kg/kWe with the current catalysts and 0.3 kg/kWe if

Table 4
Heat loads and heat exchanger sizes

	HTM (atmospheric condenser)		LTM (atmospheric condenser)		Compact HTM (pressurized condenser)		Compact LTM (pressurized condenser)	
	Q (kW)	W (kg)	Q (kW)	W (kg)	Q (kW)	W (kg)	Q (kW)	W (kg)
Fuel processor	23.7	18.3	33.4	33.9	22.1	16.2	36.1	34.6
Air heater	6.4	4.8	6.4	4.9	6.8	5.1	6.3	4.9
Steam raising	15.3	8.8	24.9	26.7	13.6	6.2	27.6	27.5
Steam superheater	5.3	4.4	5.4	4.3	5.0	4.0	5.9	4.5
HTS and boiler	4.7	1.3	5.1	0.9	4.0	0.6	5.5	1.1
LTS and economizer	3.2	2.2	5.1	4.3	3.3	1.5	5.2	5.1
PROX and reformate cooler	2.1	0.9	9.3	17.2	1.3	0.1	11.0	16.8
Fuel vaporizer	2.0	4.7	2.1	2.3	1.7	4.9	2.2	2.2
Main radiator	40.9	3.6	54.6	10.2	41.8	3.9	59.3	10.6
Water-recovery condenser	31.5	18.6	22.9	17.6	29.6	7.2	15.8	6.1
Total	96.1	40.5	110.9	61.7	93.5	27.3	111.2	51.3

target GHSVs are attained. The corresponding specific weights of the fuel processor for the LTM system are 2.8 kg/kWe with the current catalytic activities and 0.9 kg/kWe with target GHSVs. With current catalysts, the specific weight of the fuel processor is determined primarily by the activity of the catalysts. At target GHSVs, the specific weight is controlled by the heat transfer coefficients in process heat exchangers.

Table 4 also lists the heat duty and the estimated weight of the radiator that rejects waste heat from the PEFC stack. The radiator is designed for an ambient temperature of 320 K. It is air-cooled and of multi-tube, single row, finned, cross-flow construction. The fin height is between 2.5 and 3.6 times the tube diameter and the fin thickness is 0.1 mm. We assume that ram air at 320 K ambient temperature blows across the radiator at 10 m/s. The heat duty on the HTM radiator is 40.9 kW and that on the LTM radiator is 54.6 kW. The difference is because of water-condensation in the stack at 80 °C and the additional latent heat released in the process. Although the heat duty on the HTM radiator is 25% smaller, it is 65% more compact in size than the LTM radiator. The disproportionate decrease in the size of the HTM radiator results because it rejects heat from coolant water at 90 °C (selected to be 10 °C below the normal boiling point of water) whereas the coolant water in the LTM radiator is at 70 °C (10 °C approach temperature assumed in the PEFC coolant passages).

Table 4 also lists the heat duty on the water-recovery condenser. The heat load on the LTM condenser is about 27% smaller because some of the process water is recovered by phase separation in the reformate cooler and in a separator just downstream of the PEFC stack. In the high efficiency HTM system all the process water has to be recovered in the condenser. The HTM and LTM condensers are similar in construction to the radiator. The estimated weights for the condenser are 18.6 kg for the HTM system and 17.6 kg for the LTM system. In the high-performance system configuration, the condenser is located downstream of the gas turbine and operates at atmospheric pressure. It has been found that the system with an atmospheric condenser will not be water balanced at an ambient temperature of 320 K [6]. In order to ensure water balance, the condenser has been designed for an ambient temperature of 310 K.

4.2. Compact high-temperature membrane systems

One way of trimming the condenser weight is to relocate it between the PEFC stack and the tail gas burner. The condenser in this case operates at pressure so that the dew point is elevated. This means that the gas does not have to be cooled to as low a temperature as in the ambient pressure condenser and the heat duty is reduced. There is a further decrease in sensible heat load because the gas is at stack temperature rather than at turbine exit temperature. The down side is that the system efficiency suffers because the turbine inlet temperature is lower.

Simulations were conducted to analyze the performance of the system with a pressurized condenser. Fig. 15 shows the configuration analyzed for a system with a HTM stack. Both spent anode and cathode streams are being cooled in a condenser. Water self-sufficiency is obtained by cooling the streams to 58 °C. The total cooling load is 29.6 kW. These may be compared with 47 °C condenser exit temperature and 31.5 kW cooling duty at ambient pressure. Although the cooling load is only 8% lower, the reduction in the condenser size is more substantial. We calculate that the pressurized condenser weighs 7.2 kg, which is 40% of the weight of the ambient pressure condenser. At 1200 K reformer exit temperature and 2.75 atm compressor discharge pressure, the system efficiency, however, is two percentage point lower (37.3 versus 39.3% with ambient pressure condenser, see Table 5).

We have also simulated the performance of a LTM system with a pressurized condenser. For water self-sufficiency the spent anode and cathode streams must be cooled to 48 °C and 15.8 kW of heat must be rejected in the condenser. We calculate that the air-cooled cross-flow condenser will weigh 6.1 kg. For comparison, the ambient pressure condenser has a cooling load of 22.9 kW and weighs 17.6 kg. At 1200 K reformer exit temperature and 3.5 atm compressor discharge pressure, the overall efficiency of the LTM system with a pressurized condenser is 36.5% which is 1.3 percentage

Table 5
Summary of performance and specific weights of the HTM and LTM systems

	High-performance HTM	High-performance LTM	Pressurized condenser HTM	Pressurized condenser LTM
Reformer exit temperature (K)	1200	1200	1200	1200
Compressor discharge pressure (atm)	2.75	3.5	2.75	3.5
Water-to-fuel ratio in fuel processor (wt)	2.0	3.0	2.0	3.0
System efficiency (%)	39.3	37.8	37.3	36.5
Specific weights (kg/kWe)				
Fuel processor (current/target GHSVs)	1.6/0.5	2.7/0.9	1.6/0.5	2.7/0.9
Radiator	0.06	0.3	0.06	0.3
Condenser	0.4	0.4	0.2	0.2
Total	2.1/1.0	3.3/1.5	1.8/0.7	3.1/1.3

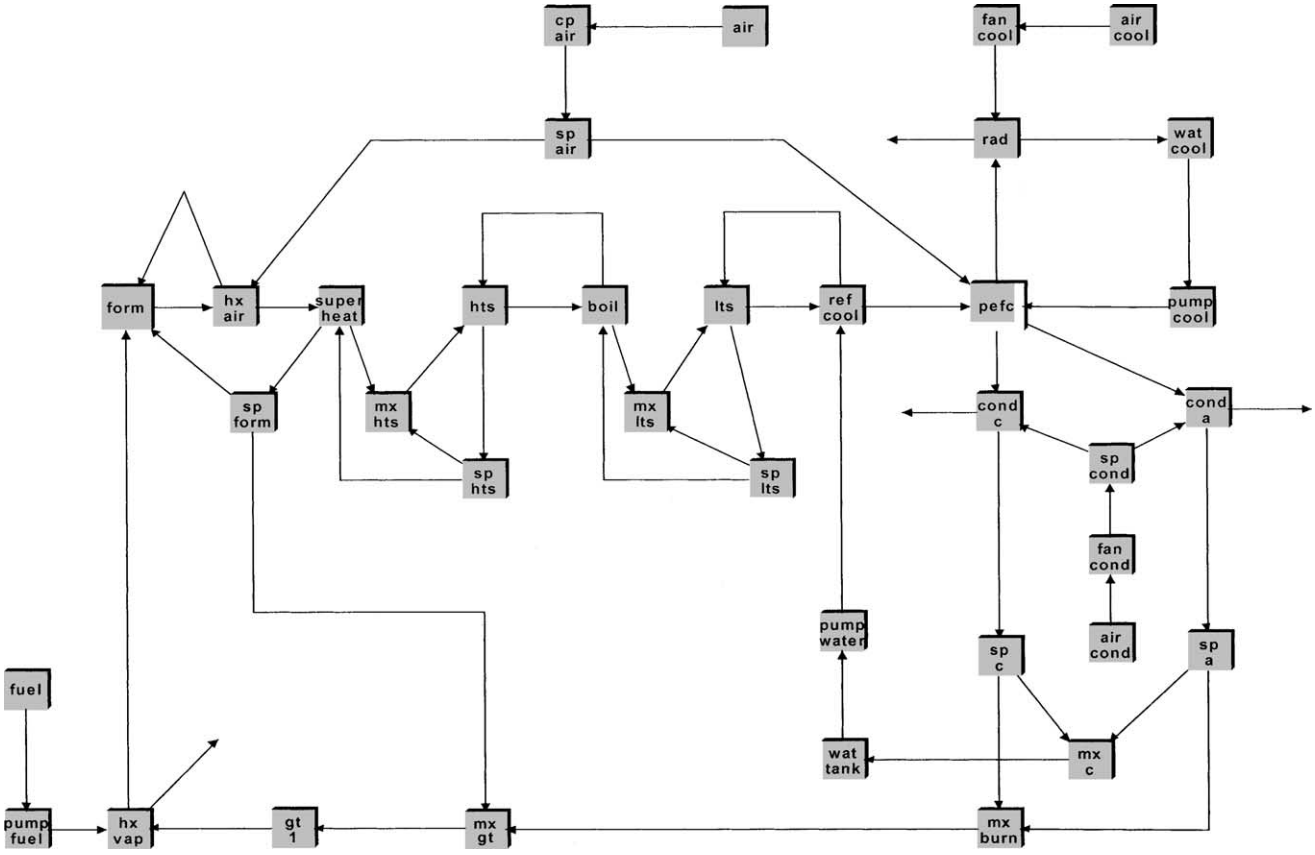

Fig. 15. Compact gasoline reformed PEFC system with a high-temperature membrane.

point lower than the equivalent system with the condenser placed after the gas turbine (see Table 5).

5. Discussion and conclusions

We have analyzed the performance of high-temperature membrane, polymer electrolyte fuel cell systems with particular attention paid to the effects of the water-to-fuel ratio in the fuel processor, fuel reforming temperature, operating pressure and stack temperature. Our simulations show that for a given reformer exit temperature, there is a water-to-fuel ratio at which the overall system efficiency is maximum. The optimum water-to-fuel ratio decreases with the reformer exit temperature, as does the overall system efficiency. For a specified reformer exit temperature, there also exists an optimum operating pressure at which the system efficiency is highest. The optimum pressure decreases slightly with the reforming temperature. Within the narrow stack temperature range of 150–200 °C considered in this study, the system efficiency improves with the stack temperature.

We summarize the principal results of our study by presenting Table 5 which lists the efficiency and specific weight attributes of a 150 °C HTM system and compares them with those of an 80 °C LTM system. Results are given for both high-performance (atmospheric condenser) and compact (pressurized condenser) configurations at 1200 K reforming temperature, a cell potential of 0.7 V and other parameters listed in Table 2. Under these conditions, the high-performance HTM system yields an overall efficiency of 39.3%. With current GHSVs, the combined specific weight of the fuel processor, radiator and the condenser is estimated as 2.1 kg/kWe. The fuel processor and the condenser account for more than 95% of the specific weight. If the target GHSVs are attained, the specific weight can be lowered to 1.0 kg/kWe.

The high-performance LTM system has an overall efficiency of 37.8%. Compared to the high-performance HTM system, the efficiency is 1.5 percentage point lower and the specific weight is about 50% higher depending on the actual GHSVs reached in the fuel processor. The radiator is almost three times the size, the fuel processor is 70–80% bulkier, but the condenser is slightly lighter.

The HTM system can be made compact by relocating the condenser between the stack and the tail gas burner. A pressurized condenser is about 60–65% lighter than an ambient pressure condenser. The combined specific weight of the fuel processor, radiator and the condenser for the compact HTM system is estimated to be 2.1 kg/kWe with current GHSVs and 1.0 kg/kWe with the target GHSVs. Thus, the compact HTM system can be almost 15–40% lighter than its high-performance version. However, the saving in the total

system weight is achieved at the expense of the overall system efficiency, which is inferior by nearly 2 percentage points.

Also, Table 5 lists the attributes of a compact LTM system. It is 6–13% lighter than its high-performance version, while its overall efficiency is 1.3 percentage point lower. Compared to the compact HTM system, the efficiency is inferior by 0.8 percentage point and the specific weight is higher by 70–85%.

References

[1] Arthur D. Little Inc., Cost Analysis of Fuel Cell System for Transportation–Baseline System Cost Estimate, Tasks 1 and 2, Final Report to DOE, Little Inc., Cambridge, MA, March 2000.

[2] R.K. Ahluwalia, et al., Performance of hydrogen fuel cell systems and vehicles, in: Proceedings of the IEA Annex XV Meeting, Dusseldorf, Germany, June 21–22, 2002.

[3] R. Kumar, E.D. Doss, R.K. Ahluwalia, H. Geyer, M. Krumpelt, Design considerations for developing efficient fuel cell systems, in: Proceedings of the IEA Annex Meeting, Argonne, IL, October 21–22, 1999.

[4] H. Geyer, R.K. Ahluwalia, GCtool for Fuel Cell Systems Design and Analysis: User Documentation, Report No. ANL-98/8, Argonne National Laboratory, Argonne, IL, March 1998.

[5] E.D. Doss, R. Kumar, R.K. Ahluwalia, R. Krumpelt, Fuel processor for automotive fuel cell systems: a parametric analysis, J. Power Sources 102 (2002) 1–15.

[6] R.K. Ahluwalia, H. Geyer, E.D. Doss, R. Kumar, System level perspective on fuel cell air management, in: Proceedings of the Fuel Cell Air Management Workshop, Argonne National Laboratory, October 10–11, 2000.